The Role of Sulfuric Acid in Atmospheric Nucleation

Mikko Sipilä, *et al.*

Science **327**, 1243 (2010);
DOI: 10.1126/science.1180315

pect (*10*). Moreover, because there are no robust paleolatitude constraints on these rocks, the Kaigas glaciation may have been regional in extent. Previous Sturtian synglacial constraints at ~685 Ma were reported from Idaho (*31*, *32*). However, these results have been questioned because the glacial nature of these deposits is uncertain, contacts between dated volcanic rocks and diamictites are tectonic, and repeated analyses have given different results (*10*). A ^{206}Pb-^{238}U ID-TIMS date of 711.52 ± 0.20 Ma was reported from volcaniclastic rocks interbedded with glacigenic deposits within the Ghubrah Formation in Oman (*27*). Thus, if the Ghubrah Formation is recording the same glacial episode as the UMHG, the Sturtian glaciation lasted a minimum of 5 million years.

Using a recalibrated and expanded $\delta^{13}C$ record, we can place the record of eukaryotic evolution in the context of geochemical perturbations and global glaciation (Fig. 2). The tuff dated at 811.5 Ma provides a maximum constraint on the Bitter Springs isotopic stage (*3*) and a useful benchmark for the calibration of early Neoproterozoic microfossil record. For instance, the chemostratigraphic position of the mineralized scale microfossils in the Lower Tindir Group of the western Ogilvie Mountains is above the Bitter Springs isotopic stage and below glacial deposits with banded iron formation that were previously correlated with the Rapitan Group (*13*). The Tindir microfossils are thus broadly coeval with complex microbiota described from the Chuar Formation in the Grand Canyon (older than 742 ± 6 Ma), the preglacial Beck Spring Formation of Death Valley, and the Svanbergfjellet Formation of Spitsbergen (*11*). Collectively, the calibration of these diverse microfossil records indicates that between the onset of the Bitter Springs isotopic stage (~811.5 Ma) and the Sturtian glaciation (~716.5 Ma), many major eukaryotic crown groups—members of Rhizaria, Amoebozoa, green and red algae, and vaucheriacean algae—had diverged and diversified. In contrast, the microfossil record between the Sturtian glaciation and the Marinoan glaciation (i.e., between ~716.5 and ~635 Ma) is depauperate; only simple acritarchs of unknown phylogenic affinity have been described (*4*, *11*). This apparent bottleneck might be due in part to poor preservation and limited sampling, and/or the survival of some groups as cryptic forms. It is clear that a diverse biosphere persisted through the Neoproterozoic glaciations (*4*), but the impact of global glaciation on eukaryotic evolution remains unresolved.

With high-precision ages directly tied to the stratigraphic record we can begin to address the mechanisms behind Neoproterozoic environmental change. The presence of the Islay $\delta^{13}C$ anomaly in the pre-Sturtian LMHG suggests a relationship between global carbon cycling and climate degradation (Figs. 1 and 2). Moreover, the synchrony among continental extension, the Franklin LIP, and the Sturtian glaciation is consistent with the hypothesis that the drawdown of CO_2 via rifting and weathering of the low-latitude Franklin basalts could have produced a climate state that was more susceptible to glaciation (*25*, *33*). However, even with the updated age constraints, it is unclear whether the bulk of the magmatism preceded or occurred during the glaciation.

References and Notes

1. J. L. Kirschvink, in *The Proterozoic Biosphere*, J. W. Schopf, C. Klein, Eds. (Cambridge Univ. Press, Cambridge, 1992), pp. 51–52.
2. P. F. Hoffman, A. J. Kaufman, G. P. Halverson, D. P. Schrag, *Science* **281**, 1342 (1998).
3. G. P. Halverson, in *Neoproterozoic Geobiology and Paleobiology*, S. Xiao, A. J. Kaufman, Eds. (Springer, New York, 2006), pp. 231–271.
4. A. H. Knoll, E. J. Javaux, D. Hewitt, P. A. Cohen, *Philos. Trans. R. Soc. Lond. Sec. B Biol. Sci.* **361**, 1023 (2006).
5. L. E. Sohl, N. Christie-Blick, D. V. Kent, *Geol. Soc. Am. Bull.* **111**, 1120 (1999).
6. D. A. D. Evans, *Am. J. Sci.* **300**, 347 (2000).
7. K. H. Hoffmann, D. J. Condon, S. A. Bowring, J. L. Crowley, *Geology* **32**, 817 (2004).
8. S. Zhang, G. Jiang, Y. Han, *Terra Nova* **20**, 289 (2008).
9. D. J. Condon *et al.*, *Science* **308**, 95 (2005).
10. P. F. Hoffman, Z.-X. Li, *Palaeogeogr. Palaeoclimatol. Palaeoecol.* **277**, 158 (2009).
11. See supporting material on *Science* Online.
12. P. S. Mustard, C. F. Roots, *Geol. Surv. Canada Bull. 492* (1997).
13. F. A. Macdonald, P. A. Cohen, F. O. Dudás, D. P. Schrag, *Geology* **38**, 143 (2010).
14. G. M. Yeo, *Geol. Surv. Canada Pap. 81-10*, 25 (1981).
15. G. H. Eisbacher, *Geol. Surv. Canada Pap. 77-35* (1978), p. 1.
16. C. F. Roots, R. R. Parrish, *Geol. Surv. Canada Pap. 88-2* (1988), p. 29.
17. L. M. Heaman, A. N. LeCheminant, R. H. Rainbird, *Earth Planet. Sci. Lett.* **109**, 117 (1992).
18. D. S. Jones, thesis, Harvard University (2009).
19. B. Schoene, J. C. Crowley, D. J. Condon, M. D. Schmitz, S. A. Bowring, *Geochim. Cosmochim. Acta* **70**, 426 (2006).
20. S. W. Denyszyn, D. W. Davis, H. C. Halls, *Can. J. Earth Sci.* **46**, 155 (2009).
21. R. H. Rainbird, *J. Geol.* **101**, 305 (1993).
22. J. K. Park, *Precambrian Res.* **69**, 95 (1994).
23. H. C. Palmer, W. R. A. Baragar, M. Fortier, J. H. Foster, *Can. J. Earth Sci.* **20**, 1456 (1983).
24. G. R. North, R. F. Cahalan, J. A. Coakley Jr., *Rev. Geophys. Space Phys.* **19**, 91 (1981).
25. J. Bendtsen, *Clim. Dyn.* **18**, 595 (2002).
26. C. Zhou *et al.*, *Geology* **32**, 437 (2004).
27. S. A. Bowring *et al.*, *Am. J. Sci.* **307**, 1097 (2007).
28. H. E. Frimmel, U. S. Klotzli, P. R. Siegfried, *J. Geol.* **104**, 459 (1996).
29. R. M. Key *et al.*, *J. Afr. Earth Sci.* **33**, 503 (2001).
30. B. Xu *et al.*, *Precambrian Res.* **168**, 247 (2009).
31. K. Lund, J. N. Aleinikoff, K. V. Evans, C. M. Fanning, *Geol. Soc. Am. Bull.* **115**, 349 (2003).
32. C. M. Fanning, P. K. Link, *Geology* **32**, 881 (2004).
33. Y. Donnadieu, Y. Goddéris, G. Ramstein, A. Nédélec, J. Meert, *Nature* **428**, 303 (2004).

34. We thank the Yukon Geological Survey for assistance with logistics and helicopter support, T. Petach and S. Petersen for assistance in the field, and D. Pearce and H. Yntema for preparing samples. Supported by the Polar Continental Shelf Project and NSF Geobiology and Environmental Geochemistry Program grant EAR 0417422.

Supporting Online Material

www.sciencemag.org/cgi/content/full/327/5970/1241/DC1
Materials and Methods
Figs. S1 to S4
Tables S1 and S2
References

14 October 2009; accepted 11 December 2009
10.1126/science.1183325

The Role of Sulfuric Acid in Atmospheric Nucleation

Mikko Sipilä,[1,2,3]* Torsten Berndt,[1] Tuukka Petäjä,[2] David Brus,[4,5] Joonas Vanhanen,[2] Frank Stratmann,[1] Johanna Patokoski,[2] Roy L. Mauldin III,[6] Antti-Pekka Hyvärinen,[5] Heikki Lihavainen,[5] Markku Kulmala[2,7]

Nucleation is a fundamental step in atmospheric new-particle formation. However, laboratory experiments on nucleation have systematically failed to demonstrate sulfuric acid particle formation rates as high as those necessary to account for ambient atmospheric concentrations, and the role of sulfuric acid in atmospheric nucleation has remained a mystery. Here, we report measurements of new particles (with diameters of approximately 1.5 nanometers) observed immediately after their formation at atmospherically relevant sulfuric acid concentrations. Furthermore, we show that correlations between measured nucleation rates and sulfuric acid concentrations suggest that freshly formed particles contain one to two sulfuric acid molecules, a number consistent with assumptions that are based on atmospheric observations. Incorporation of these findings into global models should improve the understanding of the impact of secondary particle formation on climate.

Nucleation of particles in the atmosphere has been observed to be strongly dependent on the abundance of sulfuric acid (H_2SO_4) (*1*–*4*). Sulfur dioxide (SO_2), the precursor of H_2SO_4, has both natural and anthropogenic sources. Anthropogenic SO_2 emissions can have large indirect effects on climate if H_2SO_4 is responsible for atmospheric nucleation, but laboratory experiments have systematically failed to reproduce ambient new-particle formation rates as well as the nucleation rate dependence on the H_2SO_4 concentration (Table 1) (*5*–*15*).

Reasons for these apparent differences have been unclear. Berndt *et al*. (*5*) reported laboratory experiments with nucleation occurring at nearly ambient concentrations of H_2SO_4 (10^7 molecules cm^{-3}), whereas other experiments (performed with H_2SO_4 produced from a liquid sample) have, until now, required much higher onset vapor concentrations (~10^9 molecules cm^{-3}) (*6*–*9*). This observation revived an old idea (*11*) that other compounds, such as HSO_5, that were formed in the OH + SO_2 reaction were responsible for nucleation (*13*). Recent experiments (*14*, *15*) with in situ–produced H_2SO_4 have also been used to support the idea that the nature of the nucleating species can differ from H_2SO_4.

Even though nucleation has been observed to occur just slightly above ambient atmospheric H_2SO_4 concentrations (*5*), none of the experiments performed to date have succeeded in producing the atmospherically relevant relation ("slope") between the nucleation rate (J) and H_2SO_4 concentration. This slope, according to nucleation theorem, corresponds to the number of molecules in critical cluster (*16*, *17*): $n_{crit} = d(\ln J)/d(\ln[H_2SO_4])$. Atmospheric observations (*2*–*4*) suggest this slope to be between 1 and 2. In contrast, the slopes obtained from the previous laboratory experiments (*5*–*15*) are in the range of 2 to 21.

Here, we report observations of H_2SO_4 nucleation in the presence of water vapor for ambient H_2SO_4 concentrations starting from 10^6 molecules cm^{-3}. Experiments were performed in the Leibniz-Institute for Tropospheric Research laminar flow tube (IfT-LFT) and in the Finnish Meteorological Institute (FMI) laminar flow tube (*17*). We used a chemical ionization mass spectrometer (CI-MS) (*18*) for H_2SO_4 measurements, a modified pulse height–analyzing ultrafine-condensation particle counter (PHA-UCPC) (*19*), and a mixing type particle-size magnifier (PSM) (*17*, *20*) for detecting particles down to ~1.3 to 1.5 nm in mobility-equivalent diameter (~1.0 to 1.2 nm mass diameter). With these instruments, a direct comparison with field measurements becomes possible because field observations typically apply a CI-MS for the H_2SO_4 measurement and because nucleation rates calculated from field data are given for particles with a mass diameter of 1 nm (*2*–*4*), which is close to our estimated smallest detectable particle size.

The growth rate of freshly nucleated particles because of H_2SO_4 condensation close to ambient concentrations is assumed to be small: ~1.5 nm h^{-1} at $[H_2SO_4] = 10^7$ molecules cm^{-3} (*21*). Even in the atmosphere, where several condensing vapors obviously participate in the growth process, total growth rates typically do not exceed 20 nm h^{-1} (*22*). Exceptions are coastal areas, where oxidation of iodine-containing organic vapors can rapidly produce large amounts of condensable matter (*23*), and also highly polluted environments of megacities (*24*). In order to grow nucleated particles from ~1 to 3 nm, which is the lowest detection limit of modern commercial condensation particle counters, high H_2SO_4 concentration and long growth times are required.

The detection efficiency of the present modified PHA-UCPC for <2-nm-diameter particles is several orders of magnitude higher than that of the state-of-art commercial particle counters (*19*). The PHA-UCPC allows also the determination of the particle size and the detection efficiency with which the particles are counted. Particles that are <2 nm in diameter are detected also with the PSM with an efficiency close to unity, allowing us to meet the challenge of slow growth. Figure 1 shows an example of a measurement series using three different counters: a commercial TSI-3025A condensation particle counter (CPC) (with a stated 50% detection limit of 3 nm) (TSI, St. Paul, MN), PHA-UCPC, and PSM. In the case of the PHA-UCPC, both raw data and detection efficiency–corrected data are depicted. The experiment was performed in the IfT-LFT using in situ–produced H_2SO_4. Within the residence time of 115 s, only a tiny fraction of particles grow to sizes detectable with the TSI-3025A CPC, which is a commonly used instrument in nucleation studies. The use of an improper counter clearly affects the apparent onset H_2SO_4 concentration needed for nucleation and also the slope $d(\ln N)/d(\ln[H_2SO_4])$, where N is the observed particle number concentration.

Nucleation rates obtained from different experiments are presented in Fig. 2. All series show similar behavior. For photolysis experiments, the H_2SO_4 concentrations are average concentrations from kinetic modeling (*12*). End concentrations measured with the CI-MS matched the modeled end concentrations well, with only some minor deviations for high concentrations and long residence times (fig. S1) (*17*). In the case of the H_2SO_4 from the liquid sample, the initial concentration measured by the CI-MS is shown. Separate fittings of $\ln(J)$ versus $\ln([H_2SO_4])$ to different data series (Fig. 2) yield slopes between 1.0 and 2.1, with an average value of 1.5. This is, to our knowledge, the first time that nucleation of H_2SO_4 from a liquid sample has been reported at concentrations in the range of 10^7 to 10^8 molecules cm^{-3}. This is also the first experiment showing the atmospherically relevant slope. It should be noted that in the experiment performed with the FMI laminar flow tube, the temperature was 25°C and relative humidity (RH) was 30%, whereas the IfT-LFT experiments were performed at the temperature of 20°C and RH of 22%. A 5°C higher temperature can probably explain the slightly smaller nucleation rates in the FMI experiment.

A slope of 2 can be explained by collision-controlled or kinetic nucleation (*10*), in which $J = K[H_2SO_4]^2$, where K is the kinetic coefficient. A slope of unity might, however, require an additional stabilizing and/or condensing vapor participating in the initial growth of the H_2SO_4 clusters, under the assumption that the role of water condensation is small. The slope of unity can also be explained by the activation of existing clusters (*25*), described by $J = A[H_2SO_4]$, where A is the activation coefficient, but we had no indication of preexisting clusters or gaseous impurities in our experiment (*17*). Application of kinetic or activation nucleation theory to our IfT data yields prefactor values of $K \approx 5 \times 10^{-14}$ cm^3 s^{-1} and $A \approx 3 \times 10^{-6}$ s^{-1}. This is consistent with ambient data, in which K ranges from 10^{-14} to 10^{-11} cm^3 s^{-1} (*2*–*4*) and A ranges between 10^{-7} and 10^{-5} s^{-1} (*2*, *4*).

The growth of the nucleated particles was also investigated. Figure 3 shows the mean particle diameter (d_p) determined with the PHA-

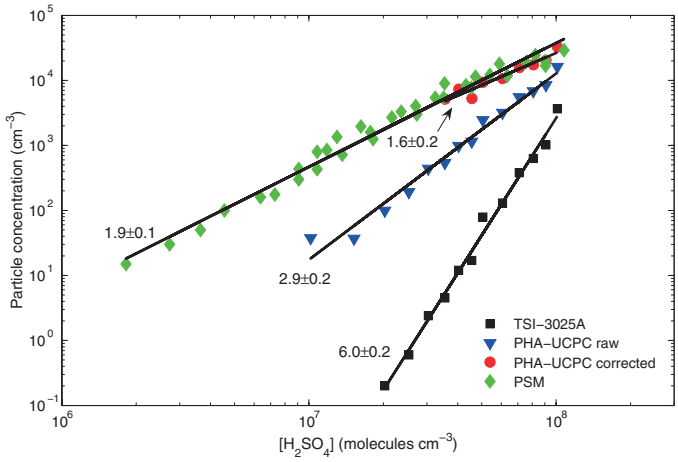

Fig. 1. Comparison of TSI-3025A, PHA-UCPC, and PSM data. In the case of PHA-UCPC, both raw data—in which the diameter-dependency of the counting efficiency is neglected—and the final, corrected data are shown. With a particle size approaching 3 nm, the different series merge. Slopes of the fittings are given in the figure. The experiment is performed in the IfT-LFT with a 115 s residence time and in situ–produced H_2SO_4. The match of the PSM data and the corrected PHA-UCPC data suggests that PSM has a close-to-unity detection efficiency for the particle size range of 1.5 to 3 nm.

[1]Leibniz-Institut für Troposphärenforschung e.V., Leipzig 04318, Germany. [2]Department of Physics, 00014 University of Helsinki, Finland. [3]Helsinki Institute of Physics, 00014 University of Helsinki, Finland. [4]Laboratory of Aerosol Chemistry and Physics, Institute of Chemical Process Fundamentals Academy of Sciences of the Czech Republic, Prague 18502, Czech Republic. [5]Finnish Meteorological Institute, Helsinki 00101, Finland. [6]National Center for Atmospheric Research, Boulder, CO 80307, USA. [7]Department of Applied Environmental Science, Stockholm University, Stockholm 10691, Sweden.

*To whom correspondence should be addressed. E-mail: mikko.sipila@helsinki.fi

UCPC for the photolysis experiments as a function of H_2SO_4 concentration for four different residence times. For comparison, the data taken with a commonly used differential mobility particle sizer (DMPS) system (with a TSI-3025A CPC) are also depicted. From the linear fittings to the data, we get an estimate of the growth rate, which is $(6 \pm 2) \times 10^{-11}$ [H_2SO_4] cm^3 molecule^{-1} nm s^{-1}. Theoretically, the growth rate from pure H_2SO_4 condensation at ~2-nm particle sizes is ~4×10^{-11} [H_2SO_4] cm^3 molecule^{-1} nm s^{-1} (*21*). The agreement can be considered good, and the small difference between measurement and theory can possibly be explained by co-condensation of water. Thus, additional condensing vapors are not necessarily needed to explain the growth in our experiments. The particle diameter after growth represents the sum of the diameter of critical cluster (d_0) and the contribution of growth. The fittings (Fig. 3) intercept the mobility diameter axis at the size d_0, suggesting a critical cluster diameter of (1.2 ± 0.2) nm, which corresponds to a mass diameter of (~0.9 ± 0.2) nm (*26*). However, it should be noted that the PHA-UCPC calibration is based on charged particles, and thus, because of the neutrality of the investigated particles, an additional positive error of ~0.3 nm can be assumed (*17*), yielding the final estimate of the critical cluster mass diameter as ~0.7 to 1.4 nm. The lower limit of this estimation corresponds to approximately 200 atomic mass units (*26*). This is reasonably well in line with our observed slope, which suggests that critical cluster probably contains up to two molecules of H_2SO_4. Furthermore, the size of critical clusters observed in our experiment is about the same as the starting size in atmospheric nucleation events (*27*).

Our experimental results regarding the onset–sulfuric acid concentration as well as the slopes for H_2SO_4 from the liquid sample are clearly in contradiction with other studies performed to date. A probable explanation for the disagreement is as follows. Our data show that high concentrations of H_2SO_4 and proper residence time are needed to allow the particles to grow to ~3 nm in diameter, which is the lowest detection limit of commercial CPCs. The detection efficiency curve of a CPC is typically very steep close to the 50% cutsize of the detector and therefore very sensitive to particle size. According to our data at RH = 22%, the growth rate was ~6×10^{-11} [H_2SO_4] cm^3 molecules^{-1} nm s^{-1}, which provides evidence that without a suitable detector and long residence times the growth of the freshly nucleated particles is not efficient enough so that they can be observed at [H_2SO_4] below ~10^8 to 10^9 molecules cm^{-3} (Fig. 3). For the most experiments performed to date, the insufficient growth rate together with insufficient counting efficiency can explain a large fraction of the discrepancy between those and our present study. To summarize, it is possible that all of the experiments cited here (including our earlier studies) have been affected either by a short residence time, size-sensitive counting efficiency of particle detectors, unexpected additional loss of H_2SO_4, or all of the above.

Explanation for the mysterious disagreement between experiments performed with in situ–produced H_2SO_4 (*5*) and H_2SO_4 from a

Table 1. Comparison of the parameters describing nucleation. The onset [H_2SO_4] for a nucleation rate of unity ($J = 1$ cm^{-3}s^{-1}) and the slope observed in the laboratory experiments using in situ–produced H_2SO_4 or H_2SO_4 from the liquid sample have previously diverged from atmospheric observations. Results of our present study match well with atmospheric observations.

	Onset [H_2SO_4] molecule cm^{-3}	Slope, d(ln)/d(ln[H_2SO_4])
Atmospheric (*1*–*4*, *28*, *29*)	~10^6	1–2
Lab, liquid sample (*6*–*9*)	10^9–10^{10}	7–21
Lab, OH+SO_2 (*5*, *10*–*15*)	10^7–10^9	2–8
This study, liquid sample and OH+SO_2	~10^6	1–2

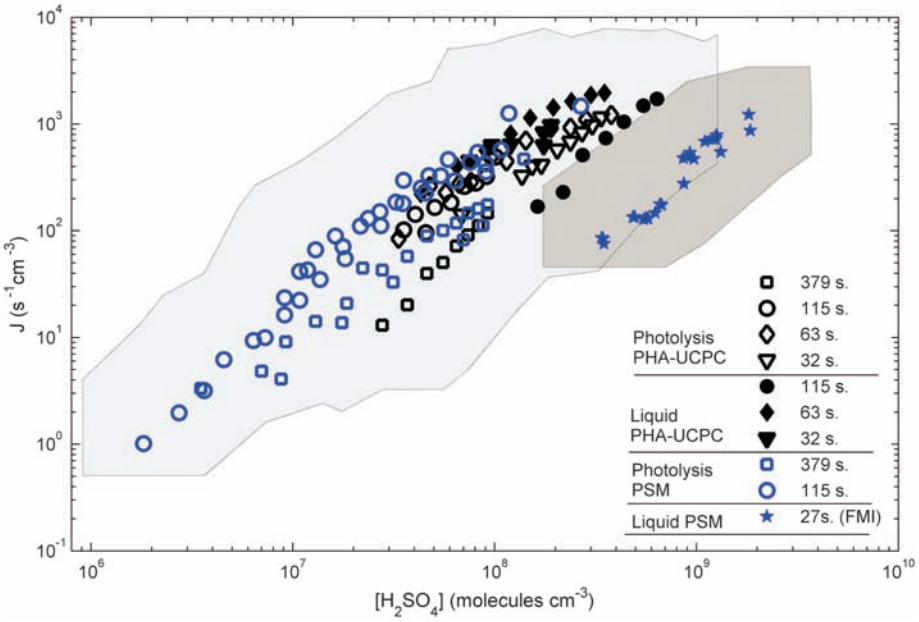

Fig. 2. Nucleation rate as a function of [H_2SO_4]. Fittings to different data series yield slopes ranging from 1.0 to 2.1 with an average slope of 1.5. The experiment in the FMI laminar flow tube was performed at +25°C and RH of 30%, whereas the data from the IfT-LFT are taken at +20°C and RH = 22%. Light and dark gray–shaded areas show the range of the error estimates in the IfT-LFT experiment and the FMI experiment, respectively. An error of (+100/–50)% for [H_2SO_4] was assumed. Error estimates in the nucleation rate comprise the inaccuracy in the determination of the nucleation zone and the error from particle counting.

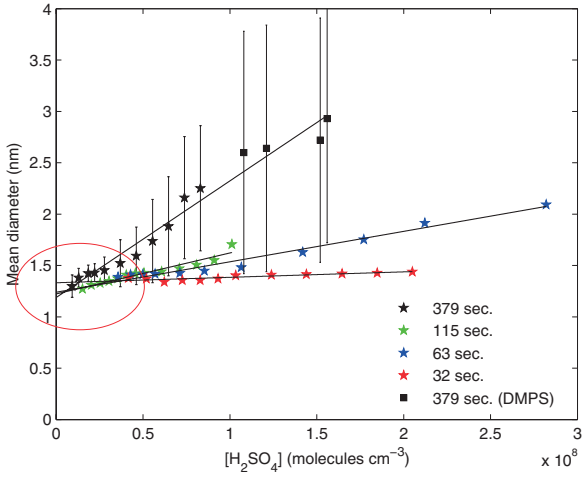

Fig. 3. Measured particle diameter for different residence times as a function of [H_2SO_4] at IfT-LFT, temperature (T) = 20°C, and RH = 22%. Data are mean mobility diameters determined with the PHA-UCPC and with the DMPS in photolysis experiments. The particle diameter is a sum of the diameter of the critical cluster and the contribution of growth. The y intercepts of the fittings suggest a critical cluster diameter of ~1.2 nm (~0.9-nm geometric diameter). Error bars represent SD of particle size distributions (for clarity, they are only shown for the 379-s series).

liquid sample (*6*–*9*) lies at least partly in the different H_2SO_4 profiles. Because of nearly uniform H_2SO_4 concentrations in case of in situ experiments (*5*, *12*, *13*), particles have much more time to grow to detectable sizes. In the case of a point source, $[H_2SO_4]$ decreases rapidly with time (fig. S3) (*17*), and the growth is not efficient enough. We have conducted experiments with these two approaches by using the same flow tube and detectors. Therefore, the differences arising from different experimental geometries and different detectors are eliminated in our study.

In conclusion, we have shown that the mystery concerning the apparent disagreement of several orders of magnitude in the nucleation rates and 2 to 3 orders of magnitude in the onset $[H_2SO_4]$ between the in situ–produced H_2SO_4 and the H_2SO_4 from a liquid sample does not exist. Therefore, the role of other sulfur-containing species (*13*), like HSO_5, seems to be of minor importance in the nucleation process, even though these other pathways cannot be completely excluded. Furthermore, we showed that nucleation occurs at atmospherically relevant H_2SO_4 concentrations. The relation between the nucleation rate and H_2SO_4 concentration $[d(\ln J)/d(\ln[H_2SO_4]) = 1.0$ to $2.1]$ from our experiment is consistent with the corresponding atmosphere observations. A nucleation rate of unity is observed at a $[H_2SO_4]$ slightly above 10^6 molecules cm^{-3}, which is well in line with most atmospheric data (*1*–*4*, *28*, *29*). However, in certain locations co-occurrence of nucleation mechanisms involving other species is plausible. We also showed that H_2SO_4 condensation has a dominating contribution to the observed particle growth in our experiment. The growth rate of $(6 \pm 2) \times 10^{-11}$ $[H_2SO_4]$ cm^3 $molecules^{-1}$ $nm\ s^{-1}$ obtained from our data is close to the theoretical estimate of pure H_2SO_4 condensation and is smaller than ambient growth rates, which supports the findings that in the atmosphere, compounds like organics (*30*, *31*) or ammonia (*32*) are involved in the early growth process. Even though the exact nucleation mechanism remains an open question, our results show that H_2SO_4 at atmospheric concentrations can explain atmospheric nucleation rates in most locations even without clear participation of ammonia or organic substances. Therefore, our findings can be used straightforwardly in further model studies, including climate models.

References and Notes

1. R. J. Weber *et al.*, *Chem. Eng. Commun.* **151**, 53 (1996).
2. S.-L. Sihto *et al.*, *Atmos. Chem. Phys.* **6**, 4079 (2006).
3. C. Kuang, P. H. McMurry, A. V. McCormick, F. L. Eisele, *J. Geophys. Res.* **113**, (D10), D10209 (2008).
4. I. Riipinen *et al.*, *Atmos. Chem. Phys.* **7**, 1899 (2007).
5. T. Berndt, O. Böge, F. Stratmann, J. Heintzenberg, M. Kulmala, *Science* **207**, 698 (2005).
6. B. E. Wyslouzil, J. H. Seinfeld, R. C. Flagan, K. Okuyama, *J. Phys. Chem.* **94**, 6842 (1991).
7. Y. Viisanen, M. Kulmala, A. Laaksonen, *J. Chem. Phys.* **107**, 920 (1997).
8. S. M. Ball, D. R. Hanson, F. L. Eisele, P. H. McMurry, *J. Geophys. Res.* **104** (D19), 23709 (1999).
9. R. Zhang *et al.*, *Science* **304**, 1487 (2004).
10. P. H. McMurry, *J. Colloid Interface Sci.* **78**, 513 (1980).
11. J. P. Friend, R. A. Barnes, R. M. Vasta, *J. Phys. Chem.* **84**, 2423 (1980).
12. T. Berndt, O. Böge, F. Stratmann, *Geophys. Res. Lett.* **33**, L15817 (2006).
13. T. Berndt *et al.*, *Atmos. Chem. Phys.* **8**, 6365 (2008).
14. L.-H. Young *et al.*, *Atmos. Chem. Phys.* **8**, 4997 (2008).
15. D. R. Benson, *Geophys. Res. Lett.* **35**, 11801 (2008).
16. D. Kashchiev, *J. Chem. Phys.* **76**, 5098 (1982).
17. Materials and methods are available as supporting material on *Science* Online.
18. F. Eisele, D. Tanner, *J. Geophys. Res.* **98**, (D5), 9001 (1993).
19. M. Sipilä *et al.*, *Aerosol Sci. Technol.* **43**, 126 (2009).
20. L. A. Sgro, J. Fernández de la Mora, *Aerosol Sci. Technol.* **38**, 1 (2004).
21. K. E. J. Lehtinen, M. Kulmala, *Atmos. Chem. Phys.* **3**, 251 (2003).
22. M. Kulmala *et al.*, *J. Aerosol Sci.* **35**, 143 (2004).
23. C. D. O'Dowd *et al.*, *J. Geophys. Res.* **107**, 8108 (2002).
24. K. Iida, M. R. Stolzenburg, P. H. McMurry, J. N. Smith, *J. Geophys. Res.* **113**, (D5), D05207 (2008).
25. M. Kulmala, K. E. J. Lehtinen, A. Laaksonen, *Atmos. Chem. Phys.* **6**, 787 (2006).
26. B. K. Ku, J. Fernández de la Mora, *Aerosol Sci. Technol.* **43**, 241 (2009).
27. M. Kulmala *et al.*, *Science* **318**, 89 (2007).
28. R. J. Weber *et al.*, *Geophys. Res. Lett.* **26**, 307 (1999).
29. W. Birmili, A. Wiedensohler, C. Plass-Dülmer, H. Berresheim, *Geophys. Res. Lett.* **27**, 2205 (2000).
30. J. N. Smith *et al.*, *Geophys. Res. Lett.* **35**, L04808 (2008).
31. C. D. O'Dowd, P. Aalto, K. Hämeri, M. Kulmala, T. Hoffmann, *Nature* **416**, 497 (2002).
32. J. N. Smith *et al.*, *J. Geophys. Res.* **110**, (D22), D22S03 (2005).

33. We thank K. Pielok and A. Rohmer for technical assistance and J. Heitzenberg, K.E.J. Lehtinen, V.-M. Kerminen, and M. McGrath for help preparing the manuscript. C. D. O'Dowd is acknowledged for providing the PHA-UCPC instrument. K. Lehtipalo is acknowledged for assistance with the PHA-UCPC, J. Mikkilä and E. Siivola for constructing the PSM, R. Taipale for help with the PTR-MS, J. Hakala and K. Neitola for assistance with experiments, and T. Nieminen for useful discussions. This work was partially funded by European Commision 6th Framework program project European Integrated Project on Aerosol, Cloud, Climate, and Air Quality Interactions (EUCAARI), contract 036833-2. Financial support from Kone foundation, Väisälä foundation, Otto Malm foundation, the Academy of Finland and European Research Council is acknowledged.

Supporting Online Material

www.sciencemag.org/cgi/content/full/327/5970/1243/DC1
Materials and Methods
SOM Text
Figs. S1 to S4

7 August 2009; accepted 5 January 2010
10.1126/science.1180315

Extensive Methane Venting to the Atmosphere from Sediments of the East Siberian Arctic Shelf

Natalia Shakhova,[1,2]*† Igor Semiletov,[1,2]* Anatoly Salyuk,[2] Vladimir Yusupov,[2] Denis Kosmach,[2] Örjan Gustafsson[3]

Remobilization to the atmosphere of only a small fraction of the methane held in East Siberian Arctic Shelf (ESAS) sediments could trigger abrupt climate warming, yet it is believed that sub-sea permafrost acts as a lid to keep this shallow methane reservoir in place. Here, we show that more than 5000 at-sea observations of dissolved methane demonstrates that greater than 80% of ESAS bottom waters and greater than 50% of surface waters are supersaturated with methane regarding to the atmosphere. The current atmospheric venting flux, which is composed of a diffusive component and a gradual ebullition component, is on par with previous estimates of methane venting from the entire World Ocean. Leakage of methane through shallow ESAS waters needs to be considered in interactions between the biogeosphere and a warming Arctic climate.

The terrestrial and continental shelf regions of the Arctic contain a megapool of carbon in shallow reservoirs (*1*–*3*), most of which is presently sequestered in permafrost (*4*, *5*). Sustained release of methane (CH_4) to the atmosphere from thawing Arctic permafrost is a likely positive feedback to climate warming (*5*, *6*). Arctic CH_4 releases are implied in both past climate shifts (*7*, *8*) and the renewed growth of contemporary atmospheric CH_4 (*9*, *10*). Observed Arctic warming in early 21st century is stronger than predicted by several degrees (fig. S1A) (*11*–*14*), which may accelerate the thaw-release of CH_4 in a positive feedback. Investigations of Arctic CH_4 releases have focused on thawing permafrost structures on land (*2*, *4*–*6*, *15*, *16*) with a scarcity of observations of CH_4 in the extensive but inaccessible East Siberian Arctic Seas (ESAS), where warming is particularly pronounced (fig. S1A) (*11*).

The ESAS (encompassing the Laptev, East Siberian, and Russian part of the Chuckchi seas) occupies an area of 2.1×10^6 km^2, three times as great as that of terrestrial Siberian wetlands. It is a shallow seaward extension of the Siberian tundra that was flooded during the Holocene transgression 7 to 15 thousand years ago (*17*, *18*). The ESAS sub-sea permafrost (fig. S1B), which is frozen sediments interlayered with the flooded peatland (*18*), not only contains comparable amounts of carbon as still land-fast permafrost in the Siberian tundra but also hosts permafrost-related seabed deposits of CH_4 (*19*). Moreover, ESAS sub-sea